Development of a numerical model of sea ice for biogeochemical studies. Part 1: Sea-ice thermodynamics

(Short title: A sea ice model for biogeochemistry: Part 1)

Letizia Tedesco[1)2)], Marcello Vichi[1)3)], Jari Haapala[4)] and Tapani Stipa[4)]

1) Centro Euro-Mediterraneo per i Cambiamenti Climatici (CMCC), Bologna, Italy
2) Centro Interdipartimentale di Ricerca per le Scienze Ambientali (CIRSA), University of Bologna, Ravenna, Italy
3) Istituto Nazionale di Geofisica e Vulcanologia, Bologna, Italy
4) Finnish Institute of Marine Research, Helsinki, Finland

A fully prognostic 1-D thermodynamic model, functional for studies of sea-ice biogeochemistry is developed to better understand the physical processes and the interactions between the environment and the sea-ice ecosystem. The physical model is capable of simulating seasonal changes of snow and ice thickness. Particular attention is paid to reproduce the snow-ice and the superimposed ice formation which play important roles in the dynamics of sea ice algae. The assessment of the model capabilities is done in 1979--1993 at four different stations in the Baltic Sea. A sensitivity analysis stresses the importance of adequate surface forcing functions to properly simulate the onset of sea ice. Our results show that thickness of the ice layers and timing of the melting are in good agreement with the observed data and confirm that one of the key variables in modelling sea-ice thermodynamics is the snow layer and its metamorphism.

1. Introduction

Though sea ice is only a very thin layer between the ocean and the atmosphere, it plays an important role in the Earth's climate system. The high albedo and its positive feedback, the strong insulating effect, the physical barrier that it creates between the atmosphere and the ocean and its impact on the large-scale thermohaline

structure of water masses make sea ice an active component of the climate system. It is thus likely that sea ice acts as a very sensitive indicator of global climate change (Eicken, 2003).

Evolution of the pack ice is driven by the heat, radiation and momentum exchanges between the ocean and the atmosphere, which can be decomposed in thermodynamic (thermal growth/decay) and dynamic processes (drift, lead openings, ridging). In the coastal fast-ice regions, sea-ice evolution is determined fully by thermodynamic processes.

The first attempt to study sea-ice thermodynamics was the analytical model developed by Stefan (1891). Later, Untersteiner (1964) and Maykut and Unterstainer (1971) moved to rather complex numerical modelling and Semtner (1976) simplified their model for numerical investigation of climate. Leppäranta (1983) introduced also snow compaction and snow-ice formation in his numerical simulations. Cox and Weeks (1988) began to study the thermal role of brines. Later Cheng *et al*. (2006) modelled the superimposed ice formation during melting periods. During the last decades other variations of such numerical models have been developed, with different complexity which aimed at different applications from the smallest to the largest temporal and spatial scales. However, not much effort has been done to analyse the properties of sea-ice thermodynamic modelling from a biogeochemical perspective.

The sea-ice ecosystem is still poorly understood. This is due to scarcity of observations, difficulties in sampling and complexity of interactions between environmental factors and sea-ice biota (Arrigo *et al.*, 1997). During ice-covered periods, sea ice algae are, potentially, the only source of fixed carbon and can support secondary production (Arrigo, 2003). Furthermore, sea ice algae are also closely related to their phytoplankton counterpart in terms of timing, magnitude and duration of the blooms (Gosselin *et al*. 1997). The inclusion of sea-ice ecosystem dynamics in Earth System Models (ESM) may be an important feature to complete the carbon cycle closure in the polar and sub-polar regions. Modelling the sea-ice

biogeochemistry is thus a valuable tool to better understand the fate of this biomass, its contribution to the total primary production and their role in the global carbon cycle.

Temperature, salinity, space, nutrients and light availability are the main environmental factors that affect the growth, the distribution and the abundance of sea ice algae. At the bottom of the ice sheet, temperature, salinity, space and nutrients are more favourable to sea ice algae growth, but primary production is often limited by thick snow covers that prevent a sufficient penetration of light. The situation is opposite on top of the ice sheet. Snow ice and superimposed ice play important roles, not only because they change the snow properties and the consequent rates of ice growth, but also because they create suitable habitats for sea ice algae, bringing nutrients where the light is more available.

To estimate the total fraction of primary production in sea ice, it is required to model sea ice algae growth in every different physical layer of the ice sheet. To date, very few efforts have been done to develop a coupled physical-biogeochemical model of sea ice that it is also suitable to be efficiently coupled with physical-biogeochemical ocean models and ultimately with ESMs.

After the pioneering work of Arrigo *et al*. (1993), only recently there have been further attempts to model the biomass of the ice sheet (Nishi and Tabeta 2005; Jin *et al*. 2006). Arrigo *et al*. (1993) coupled a relative complex model of microalgal growth with a very simple first-year sea-ice thermodynamic model. Nishi and Tabeta (2005) used a 10-layer Maykut-Untersteiner thermodynamic sea ice model and they limited their model to reproduce the biomass in the last centimetres of the ice sheet. Jin *et al*. (2006) modelled the bottom algal community in the last two centimetres of the ice sheet, while snow and ice data were provided from observations.
In this first paper, we present the initial implementation of a fully prognostic 1-D thermodynamic model that can be functional for studies of sea-ice biogeochemistry. In the second step, we will analyse the direct coupling with an improved version of

the Biogeochemical Flux Model (BFM, Vichi et al., 2007a,b) capable of simulating the fraction of total primary production in the different layers of ice.

2. Description of the physical model

Following Semtner 0-layer model (Semtner, 1976), the sea-ice system consisted of one layer of ice and one layer of snow on top. The model is developed is such a way that, depending on the required complexity, more layers of sea ice can be added and simulated. Prognostic variables included two layers of snow (two density classes), three layers of ice (superimposed ice, snow ice and sea ice), temperature at the surface and analytically at the interfaces. A schematic drawing of the model is presented in Fig. 1. Table 1 presents the values of the model parameters. In all the following equations the subscript *s* indicates snow, *i* ice, *sn* snow ice, *ss* superimposed ice and *si* sea ice, while the subscript *mi* refers to snow ice and superimposed ice together. The model code is freely available for download in the BFM website (http://www.bo.ingv.it/bfm).

A 1-dimensional heat conduction equation governed the vertical heat fluxes at the boundaries and between the different layers. Snow and ice temperatures were given by

$$(\rho\, c)_{i,s} \frac{\partial T_{i,s}(z,t)}{\partial t} = \frac{\partial}{\partial z}\left(k_{i,s} \frac{\partial T_{i,s}(z,t)}{\partial z} \right) \quad (1)$$

where ρ is the density, c is the heat capacity, T is the temperature and k is the thermal conductivity. When sea ice was the only layer of the ice sheet, the sea-ice temperature equation differed for the presence of the penetrating solar radiation which depends on the albedo α and on the extinction coefficient κ

$$(\rho\, c)_{si} \frac{\partial T_{si}(z,t)}{\partial t} = \frac{\partial}{\partial z}\left(k_{si} \frac{\partial T_{si}(z,t)}{\partial z} \right) + (1-\alpha_{si}) F_s\, e^{-\kappa_{si} z} \quad (2)$$

where F_s is the incoming solar radiation.

The different layers were supposed to be in thermal equilibrium and the temperatures at the interfaces were derived from the continuity of the heat fluxes

$$\frac{\partial}{\partial z}\left(k_i \frac{\partial T_i(z,t)}{\partial z}\right) = \frac{\partial}{\partial z}\left(k_s \frac{\partial T_s(z,t)}{\partial z}\right) \quad (3).$$

The surface temperature T_0 was obtained by linearly approximating the surface fluxes F, expanding in a Taylor series and iterating according to the Newton-Raphson method for twenty times with a convergence criterion of maximum one Kelvin between consecutive time steps

$$T_0^{\,n+1} = T_0^{\,n} - \frac{F\left(T_0^{\,n}\right)}{F'\left(T_0^{\,n}\right)} \quad (4).$$

Different albedo values were used during the growth and melting seasons depending on the snow or ice type at the surface (see Table 1). Snow accumulated on top of the layers whenever the temperature of the air was under the freezing point of snow and an ice layer was already present. If young fallen snow $(h_s)_y$ accumulated on an already present snow layer, snow compaction was initiated

$$h_s = (h_s)_y \frac{(\rho_s)_y}{\rho_s} \quad (5).$$

The total surface fluxes F included shortwave (F_s) and longwave radiation (F_l), sensible (F_{se}) and latent heat (F_{la}). At the surface snow, snow ice, superimposed ice and sea ice melted whenever the surface temperature was at the melting point and the rate of melting was determined by the net heat flux balance between the surface fluxes and the conductive fluxes

$$\left(-k_{i,s}\frac{\partial T_{i,s}}{\partial z}\right)_{surf}+(1-\alpha_{i,s})F_s-(1-\alpha_i)F_s\,e^{-\kappa_i z}+F_l+F_{se}+F_{la}=-\rho_{i,s}(L_f)_{i,s}\frac{dh_{i,s}}{dt}\quad(6)$$

where L_f is the latent heat of fusion.

If the surface heat fluxes exceeded the conductive fluxes, the imbalance in the surface energy budget contributed to increase the conductive flux of the surface layer and the surface energy balance changed to

$$\left(-k_{i,s}\frac{\partial T_{i,s}}{\partial z}\right)_{surf}+(1-\alpha_{i,s})F_s-(1-\alpha_i)F_s\,e^{-\kappa_i z}+F_l+F_{se}+F_{la}=0\quad(7).$$

The temperature at the bottom of the ice sheet was set constant at the freezing point of seawater. At the ice-water interface constant values ranging between 3 and 6 W/m^2 – depending on the location of the simulated station – represented the oceanic heat fluxes. At the bottom, ice either grew or melted according to the net heat flux balance between the oceanic fluxes F_w and conductive fluxes

$$-\rho_i(L_f)_i\frac{dh_i}{dt}=\left(-k_i\frac{\partial T_i}{\partial z}\right)_{bot}+F_w\quad(8).$$

As originally proposed in Fichefet and Morales Maqueda (1999), if the ice draft exceeded the ice thickness, i.e.

$$\frac{h_s\rho_s-h_{sn}(\rho_w-\rho_{sn})}{(\rho_w-\rho_{si})}\rangle\, h_{si}\quad(9)$$

then snow-ice formation was initiated. Snow density and compaction were changed accordingly and a new isostatic equilibrium was prescribed. No seawater mass was added and snow was compressed to an amount of new snow ice equal to the initial depression below the water line (Schmidt *et al*. 2004)

$$h_{sn} = \frac{\rho_s\ h_s + (\rho_{si} - \rho_w)\, h_{si} + (\rho_{mi} - \rho_w) h_{mi}}{\rho_w - \rho_{mi} + \beta\ \rho_s} \quad (10)$$

$$h_s = (h_s)_y - \beta\left(h_{sn} + \frac{(\rho_s)_y\,(h_s)_y}{\rho_w + \beta\,\rho_s - \rho_{mi}} \right) \quad (11)\,.$$

where β is an empirical coefficient of conversion between snow ice and sea ice (after Leppäranta, 1983). Snow ice melted according to the same energy balance previously described in Eq. 6.

If melted snow re-freezed under positive temperature gradient within the snow and ice layers, superimposed ice formation was also initiated by transforming a fraction of snow, depending on snow properties, in superimposed ice, as in Cheng *et al.* (2006)

$$h_{ss} = (h_s)_{melt}\,\frac{\rho_s}{\rho_{ss}} \quad (12)\,.$$

3. Experiment design and methods

In order to validate the modelled seasonal evolution of the snow, snow-ice, superimposed ice and sea-ice thickness and examine inter-annual variability of the thermal growth of sea ice, the regular sea-ice observations were used for a comparison. The model was implemented in the Baltic Sea at four different stations (Fig. 2): Ajos (65° 39.8’ N, 24° 31.4’ E), Kummelgrund (62° 09.3’ N, 21° 09.5’ E), Jussarö (59° 53.4’ N, 23° 31.1’ E) and Kotka (60° 27.3’ N, 26° 57.2’ E). Ajos is the northernmost station and it is characterized by the most severe winters, more ice formation, snow accumulation, snow-ice formation and faster melting with minor superimposed ice growth. Jussarö is the southernmost station and it is characterized by less severe winter, less sea-ice growth and snow precipitation, thought consistent superimposed ice grows during the melt period. Kummelgrund is latitudinally

located between Ajos and Jussarö and has intermediate characteristics between the two. Kotka is the easternmost station and shows similar characteristics to Jussarö, but since it is located north of Jussarö the area is affected by higher sea-ice growth rate.

The meteorological data were taken from ECMWF ERA-15 6h Reanalysis data at 2.5 degrees resolution (Gibson *et al.* 1997) considering air temperature at 2 m height, total cloud cover, wind speed at 10 m height, large scale precipitation and convective precipitation. Due to biases in the ERA-15 database, we used NCEP 6h Reanalysis (Kalnay *et al*. 1996) for irradiance and specific humidity at the surface and at 2 m height. The weekly observations of snow, snow-ice, superimposed ice and sea-ice thicknesses were provided by the Ice Service at the Finnish Institute of Marine Research. The chosen simulation period was 1979--1993.

The choice of such a coarse resolution database was driven by the plans of using this model also in coupled configurations within ESMs. To assess the sensitivity of the model to the resolution of the forcing data, we performed a sensitivity analysis to one of the test-case station by adding a random white noise based on the spatial standard deviation of the meteorological data around the station point. To quantify the skill of the model in the short and long terms, we computed the timeseries of Root Mean Square Errors (RMSE) between the model standard run and the perturbed simulation against the observations

$$RMSE = \sqrt{\frac{1}{n}\sum_{j=1}^{n}\left(x_m - x_o\right)^2} \quad (13)$$

where n is the number of comparisons, x_m is the standard/perturbed model value and x_o is the observation value.

We also computed the normalized Root Mean Square Error (nRMSE) to obtain a measure of the relative error in time and to better highlight the model skills and the major weaknesses in a key period for sea ice algae development such as the sea-ice formation

$$nRMSE = \sqrt{\frac{1}{n}\sum_{j=1}^{n}\left(\frac{x_m - x_o}{x_o}\right)^2} \quad (14)$$

Finally, we challenged the model structure by performing a classical sensitivity test to precipitations, prescribing fixed variations proportional to the observed standard deviation of data.

4. Simulation results

In Fig. 3 and Fig. 4 we show the simulation results of the thicknesses plotted against observations at every station. The two types of snow are grouped together (*hs*) and plotted in the positive ordinate. Snow ice and superimposed ice are also grouped together as an intermediate layer (*hmi*) and plotted in the negative ordinate. The total ice thickness (*hi tot*) is shown in the negative ordinate as the sum between the intermediate layer and the sea-ice thickness.

The model seemed to reproduce well the dominant physical features of the ice sheet (Fig. 3 and Fig. 4): the timing of melting and the thickness of the ice layers were in general good agreement with observations at all stations, except few cases – for example in Ajos, Kummelgrund and Kotka during the ice season 1984--1985 –. On the contrary, the model generally underestimated the maximum thickness of the snow layer, especially in Ajos station – for example during the ice seasons 1979--1980, 1980--1981 and 1987--1988. This is probably due to the fact that snow compaction is initiated when new precipitation falls on old snow. However, since the total weight of snow on ice was conserved, the mismatch between simulations and observations did not affect the total ice thickness. Besides, the timing of the sea-ice growth seemed sometimes ahead of the observed beginning of the sea ice season, particularly in Ajos station – for example in the ice seasons 1979--1980, 1982--1983 and 1984--1985 –. Ajos is characterized by higher ice growth rates and usually presents all the ice types considered. The model showed to be here more sensitive to

the lower surface temperatures and higher precipitation rates and for this reason we focused our analysis on this station and we performed different sensitivity tests in here.

5. Sensitivity analyses and discussion

Our first test aimed to objectively quantify the model skill with respect to the observations, focusing on the dependence upon the forcing data resolution. As described in Sect. Experiment design and methods, we computed the timeseries of the RMSE (Fig. 5) and nRMSE (Fig. 6) between the observations and the standard model run and between the observations and a perturbed model run in which we added a random white noise to the forcing data.

The standard run produced a final residual variation ranging between 0.088 m for snow to 0.133 m for the total ice thickness (Fig. 5). The perturbed model run always caused a larger error evolution and a final RMSE ranging between 0.091 m for snow and 0.139 for total ice thickness (Fig. 5). The difference between the two runs was especially higher for the intermediate layer (*hmi*) of snow ice and superimposed ice. Both ice types originate from snow metamorphism. As mentioned above, the model showed a generally earlier compaction, which is better shown in the nRMSE (Fig. 6) as a systematic error in time for both the snow layer and, consequently, for the intermediate layer. Even though both the RMSE and the nRMSE showed a weak final difference between the standard and the perturbed runs for the snow layer, larger errors were found in the intermediate layer, especially in the first five years of simulation. After that period, the model differences were reduced, which implies that the spatial uncertainties on the forcing data affect the long term model skills to a lesser extent.

The standard run of the model shows a steady RMSE of the total ice thickness around 0.11 m during 1979--1984, while during the ice seasons 1984--1985 and 1985--1986 the RMSE dramatically increased (Fig. 5). A closer look to the sea-ice evolution in 1984--1985 (Fig. 7) shows that sea ice began to grow earlier than

observed and snow accumulated on it later than observed. As a result, the model initially simulated more sea ice than observations. At the beginning of 1985 the trend changed. The model accumulated too large amount of snow on top of the ice sheet and the sea-ice growth rate was reduced, leading to an underestimation of the total ice thickness for the following months. During the following ice season 1985--1986 (Fig. 8), even though the timing of sea-ice formation was in good agreement with observations, snow began to accumulate much later. Consequently, the model simulated more sea-ice growth and it was not able to reach the observed thickness. Following these two ice seasons, the RMSE of the total ice thickness began to decrease again stabilising around the final value (Fig. 5).

The timeseries of the nRMSE (Fig. 6) shows that the larger relative errors are generally at the beginning of the ice seasons due to an earlier sea-ice formation. The largest ones occured during the ice seasons 1979--1980 and 1980--1981 for the total ice thickness. At the end of 1979 and 1980 (Figs. 9-10) sea ice began to grow earlier than observed and this resulted in an error increase up to 0.7 the total ice thickness in 1979--1980 and up to 0.95 in 1980--1981. However, since snow started to accumulate earlier as well, its insulating effect strongly reduced the initial sea-ice growth rate and later the model was able to correctly reach the maximum total ice thickness and the nRMSE was reduced in both cases. Also in these cases, there was a mismatch due to snow compaction. Later, minor errors propagated until 1986--1987. After this period, the thermodynamic model showed to better reproduce the total ice thickness, as during the ice season in 1986--1987 (Fig. 11) and the nRMSE decreased and stabilises until the end of the simulation period (Fig. 6).

In order to further test the sensitivity of the model to snow accumulation, we also performed the classical sensitivity test to fixed variations in the precipitation forcing. We thus forced the model with standard precipitation data plus/minus one standard (Fig. 12). Results confirmed that an increase in precipitation did not directly affect the thickness of the snow layer, but it was reflected in the timing of formation and in the thickness of the intermediate layer and, consequently, on the total ice thickness. On the other hand, reducing the amount of precipitation further underestimated the

thickness of the snow layer, which did not allow snow-ice and superimposed ice formation in any of the simulated ice seasons and generally increased the total ice thickness.

6. Conclusions and future development

In this first paper, we show that an improved version of Semtner-0 layer model reasonably reproduces the inter-annual variability of the sea ice season in the ice-covered Baltic Sea with acceptable skill scores. Some of the main physical features of the sea-ice evolution are rather well reproduced. Particularly, the thickness of the ice layers and the timing of melting are generally in good agreement with the observed data, while the timing of ice formation is sometimes earlier to observations (Fig. 6).

Coupled models and particularly ESMs generally have resolutions comparable or slightly finer than the reanalysis data used here. From the sensitivity analysis, we find that after a few years of bigger relative and absolute errors, the perturbed model run does not significantly differ from the standard run and we can then conclude that such coarse resolution of the forcing data can be acceptable for long term simulations of sea-ice thermodynamics, but not for short term forecasting.

From the more detailed analysis in Ajos (Figs. 7-11) and from the sensitivity test to precipitation (Fig. 12) , it is clear that the model does a good job whenever the snow layer is well simulated and it is not necessary to add more sea-ice layers to better reproduce the total ice thickness. The model is, instead, clearly very sensitive to snow metamorphism and snow is the key variable in sea-ice thermodynamics because of its different metamorphoses, high albedo and strong insulating effect. We believe that more attention should be paid to snow accumulation, compaction and metamorphoses to improve our results.

Model results are sufficiently robust for an appropriate simulation of the ice characteristics (timings, thicknesses and temperatures) functional to the Baltic Sea

biota, where sea-ice salinity plays a minor role, being close to 0 ‰, and usually characterized by constant vertical profile in time. Once salinity, density and brines properties, that are currently under development, will be included in the model, we will extend our applications to Arctic and Antarctic regions as well.

Acknowledgements

This study is supported by the VECTOR project, funded by the Italian Ministry of the University and the Scientific Research. Collaboration with the Finnish Institute of Marine Research has started thanks to the "Marco Polo" scholarship awarded by the University of Bologna to the first author and it is going on in the framework of EUROceans, Network of Excellence. NCEP Reanalysis and ECMWF data have been provided by the NOAA/OAR/ESRL PSD, Boulder, Colorado, USA, from their Web site at http://www.cdc.noaa.gov/. The observed snow and ice thickness data have been provided by the Ice Service at the Finnish Institute of Marine Research. We are particularly grateful to Ari Seinä for support with the observations.

References

Arrigo K.R., Kremer J.M. & Sullivan C.W. 1993. A simulated Antarctic Fast Ice Ecosystem. *J. Geoph. Res.* 98, No C04: 6929--6946.

Arrigo K.R., Worthen D.L., Lizotte P., Dixon P & Dieckmann G. 1997. Primary production in Antarctic sea ice. *Science.* 276, 394--397.

Arrigo K.R. 2003. Primary production in sea ice. In: Thomas D.N. & Dieckmann G.S. (eds.), *Sea ice: an introduction to its physics, biology, chemistry and geology*, Blackwell Science, Oxford, pp. 143--183.

Cheng B., Vihma T., Pirazzini R. & Granskog M. A. 2006. Modelling of superimposed ice formation during the spring snowmelt period in the Baltic Sea. *Ann. Glaciol*. 44, No. 1: 139--146(8).

Eicken H. 2003. From the Microscopic, to the Macroscopic, to the Regional scale: Growth, Microstructure and Properties of Sea Ice. In: Thomas D.N. & Dieckmann G.S. (eds.), *Sea ice: an introduction to its physics, biology, chemistry and geology*, Blackwell Science, Oxford, pp. 22--81.

Fichefet T. & Morales Maqueda M.A. 1999. Modelling the influence of snow accumulation and snow-ice formation on the seasonal cycle of the Antarctic sea-ice cover. *Climate Dynamics* 15: 251--268.

Gibson J. K., Kallberg P., Uppala S., Noumura A., Hernandez A., & Serrano E. 1997. ERA Description. ECMWF Re-Analysis Project Report Series, 1. ECMWF, Reading, UK, pp. 77.

Gosselin M., Levasseur M., Wheeler P.A., Horner R.A. & Booth B.C. 1997. New measurements of phytoplankton and ice algal production in the Arctic Ocean. *Deep Sea Res. II* 44, No. 8: 1623--1644.

Jin M., Deal C.J., Wang J., Shin K.-H., Tanaka N., Whitledge T.E., Lee S.H. & Gradinger R.R. 2006. Controls of landfast ice-ocean ecosystem offshore Barrow, Alaska. *Ann. Glaciol.* 44: 63--72(10).

Kalnay E., Kanamitsu M., Kistler R., Collins W., Deaven D., Gandin L., Iredell M., Saha S., White G., Woollen J., Zhu Y., Leetmaa A., Reynolds B., Chelliah M., Ebisuzaki W., Higgins W., Janowiak J., Mo K., Ropelewski C., Wang J., Jenne R. & Joseph D. 1996. The NCEP/NCAR 40-Year Reanalysis Project. *Bull. Amer. Meteor. Soc.*, 77: 437--471.

Leppäranta M. 1983. A growth model for black ice, snow-ice and snow thickness in subarctic basins. *Nordic Hydrol*. 14: 59--70.

Maykut G.A. & Untersteiner N. 1971. Some results from a time dependent thermodynamic model of sea-ice. *J. Geoph. Res.* 76(6): 1550--1575.

Nishi Y., & Tabeta S. 2005. Analysis of the contribution of ice algae to the ice-covered ecosystem in Lake Saroma by means of a coupled ice-ocean ecosystem model. *J. M. S.*: 55(3-4), 249--270.

Schmidt G.A., Bitz C., Mikolajewicz U. & Tremblay L.-Bruno 2004. Ice-ocean boundary conditions for coupled models. *Ocean Modelling* 7: 59--74.

Semtner A.J. 1976. A model for the thermodynamic growth of sea ice in numerical investigation of climate. *J. Phys. Oceanogr.* 6: 379--389.

Stefan J. 1891. Über die Theorie der Eisbildung, insbesondere über Eisbildung im Polarmeere. *Ann. Phys.* 42(2): 269--286.

Untersteiner N. 1964. Calculations of temperature regime and heat budget of sea-ice in the central Arctic. *J. Geoph. Res.* 69(22): 4755--4766.

Vichi M., Pinardi N. & Masina S. 2007a. A generalized model of pelagic biogeochemistry for the global ocean ecosystem. Part I: Theory. *J. Mar. Sys*. 64, No. 1-4: 89--109.

Vichi M., Masina S. & Navarra A. 2007b. A generalized model of pelagic biogeochemistry for the global ocean ecosystem. Part II: Numerical simulations. *J. Mar. Sys*. 64, No. 1-4: 110--134.

Table 1. Sea ice model parameters.

Parameter	Physical meaning	Value	Unit
σ_a	Stefan-Boltzmann constant	5.68×10^{-8}	$W\ m^{-2}\ K$
ε	Surface emissivity	6.74×10^{-2}	---
ρ_a	Density of air	1.225	$kg\ m^{-3}$
ρ_{ns}	Density of new snow	200	$kg\ m^{-3}$
ρ_s	Density of snow	400	$kg\ m^{-3}$
ρ_{sn}	Density of snow ice	880	$kg\ m^{-3}$
ρ_{ss}	Density of superimposed ice	850	$kg\ m^{-3}$
ρ_{si}	Density of sea ice	900	$kg\ m^{-3}$
ρ_w	Density of seawater	1026	$kg\ m^{-3}$
k_{ns}	Thermal conductivity of new snow	0.056	$W\ m^{-1}\ K^{-1}$
k_s	Thermal conductivity of snow	0.180	$W\ m^{-1}\ K^{-1}$
k_{sn}	Thermal conductivity of snow ice	0.950	$W\ m^{-1}\ K^{-1}$
k_{ss}	Thermal conductivity of superimposed ice	0.900	$W\ m^{-1}\ K^{-1}$
k_{si}	Thermal conductivity of sea ice	2.000	$W\ m^{-1}\ K^{-1}$
κ_{si}	Extinction coefficient of sea ice	(1.5—17.1)	m^{-1}
s_w	Seawater salinity	(4—5.5)	ppt
c_{si}	Heat capacity of sea ice	2093	$J\ kg^{-1}\ K^{-1}$
c_{sn}	Heat capacity of snow ice	2093	$J\ kg^{-1}\ K^{-1}$
c_{ss}	Heat capacity of superimposed ice	2093	$J\ kg^{-1}\ K^{-1}$
c_s	Heat capacity of snow	2093	$J\ kg^{-1}\ K^{-1}$
c_a	Specific heat of air	1004	$J\ kg^{-1}\ K^{-1}$
c_w	Specific heat of seawater	4186	$J\ kg^{-1}\ K^{-1}$
T_f	Freezing temperature of sea ice	272.85—272.93	K
T_{f0}	Freezing temperature of snow	273.15	K
q_s	Volumetric heat of fusion of snow	132×10^6	$J\ m^{-3}$
q_{sn}	Volumetric heat of fusion of snow ice	293.92×10^6	$J\ m^{-3}$
q_{ss}	Volumetric heat of fusion of superimposed ice	293.92×10^6	$J\ m^{-3}$
q_{si}	Volumetric heat of fusion of sea ice	303.94×10^6	$J\ m^{-3}$
α_{ns}	Surface albedo of new snow	(0.75—0.85)	---
α_s	Surface albedo of snow	(0.50—0.7)	---
α_{sn}	Surface albedo of snow ice	(0.40—0.6)	---
α_{ss}	Surface albedo of superimposed ice	(0.40—0.6)	---
α_{si}	Surface albedo of sea ice	(0.25—0.5)	---
α_w	Surface albedo of seawater	0.060	---

Fig. 1. General structure of the sea ice model (heat fluxes, temperatures, snow and ice layers) during growth (left) and melt (right) periods.

Fig. 2. Location of the stations for model comparison.

Fig. 3. Observations and model simulations at Ajos (above) and Kummelgrund (below) stations in 1979--1993 (hs: snow; hmi: snow ice + superimposed ice; hi tot: total ice thickness).

Fig. 4. Observations and model simulations at Jussarö (above) and Kotka (below) stations in 1979--1993 (hs: snow; hmi: snow ice + superimposed ice; hi tot: total ice thickness).

Fig. 5. Root Mean Square Error in time between observations, standard run and perturbed run at Ajos station.

Fig. 6. Normalized Root Mean Square Error in time between observations, standard run and perturbed run at Ajos station.

Fig. 7. Observations and model simulation at Ajos station in 1984--1985.

Fig. 8. Observations and model simulation at Ajos station in 1985--1986.

Fig. 9. Observations and model simulation at Ajos station in 1979--1980.

Fig. 10. Observations and model simulation at Ajos station in 1980--1981.

Fig. 11. Observations and model simulation at Ajos station in 1986--1987.

Fig. 12. Sensitivity of the model to increased (above) and decreased (below) precipitation (Ajos).

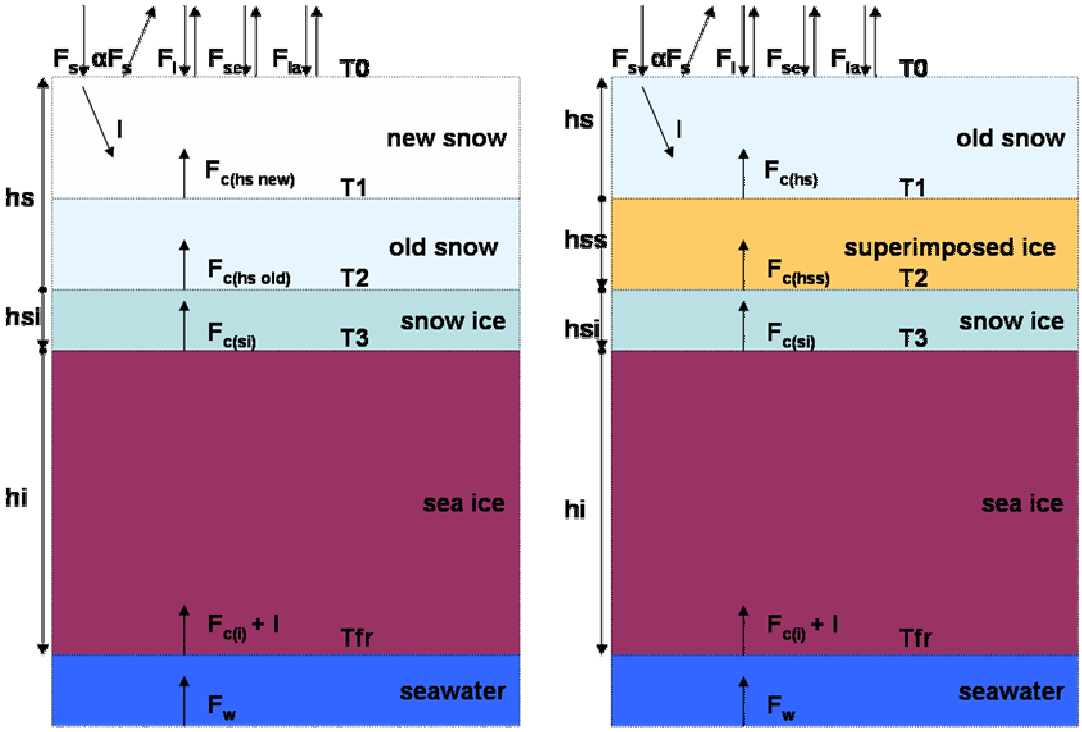

Fig. 1. General structure of the sea ice model (heat fluxes, temperatures, snow and ice layers) during growth (left) and melt (right) periods.

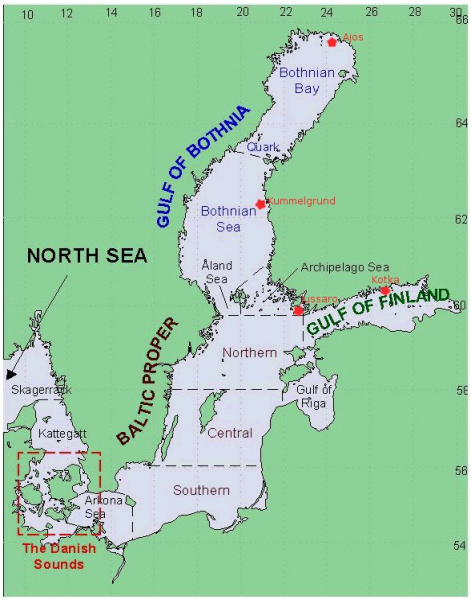

Fig. 2. Location of the stations for model comparison.

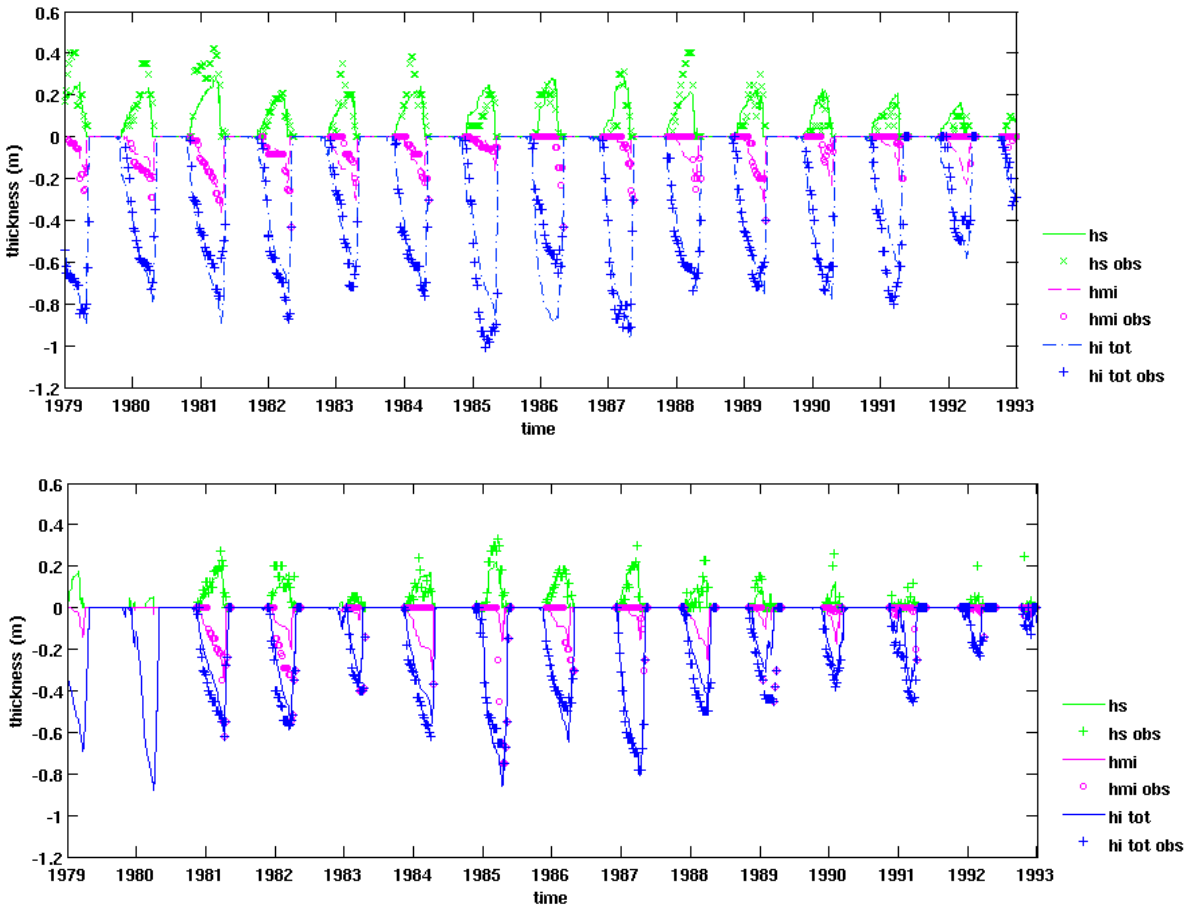

Fig. 3. Observations and model simulations at Ajos (above) and Kummelgrund (below) stations in 1979--1993 (hs: snow; hmi: snow ice + superimposed ice; hi tot: total ice thickness).

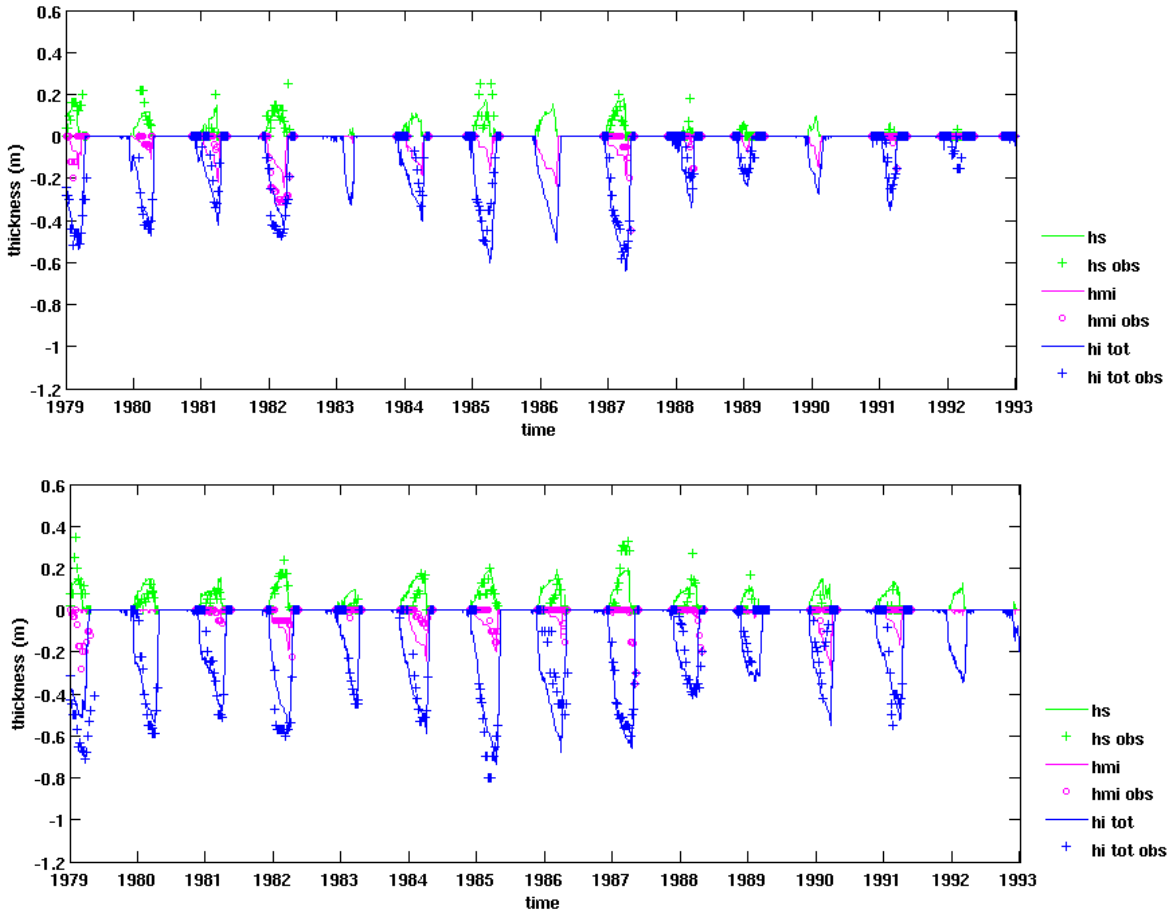

Fig. 4. Observations and model simulations at Jussarö (above) and Kotka (below) stations in 1979--1993 (hs: snow; hmi: snow ice + superimposed ice; hi tot: total ice thickness).

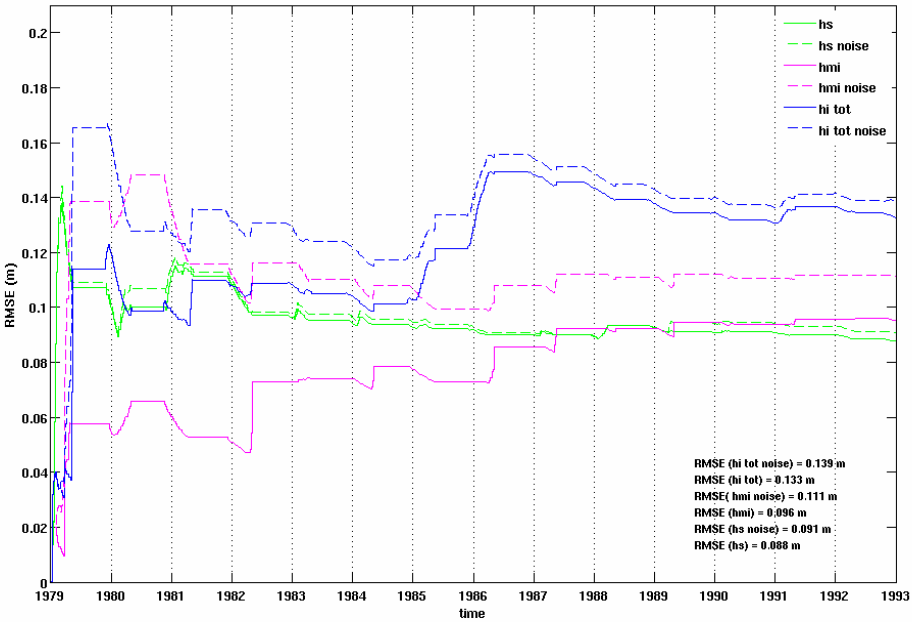

Fig. 5. Root Mean Square Error in time between observations, standard run and perturbed run at Ajos station.

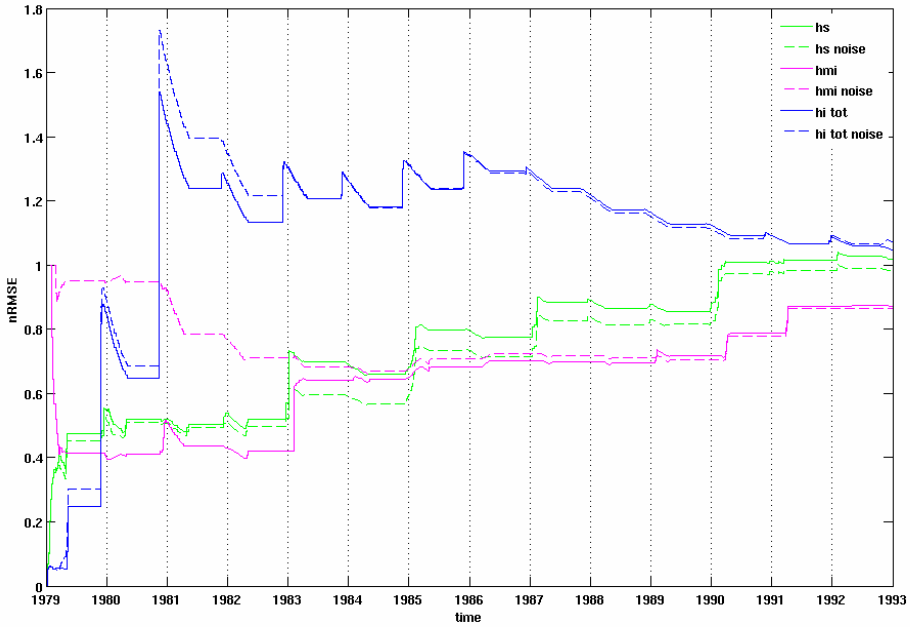

Fig. 6. Normalized Root Mean Square Error in time between observations, standard run and perturbed run at Ajos station.

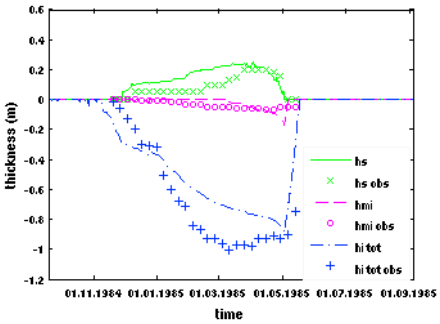

Fig. 7. Observations and model simulation at Ajos station in 1984--1985.

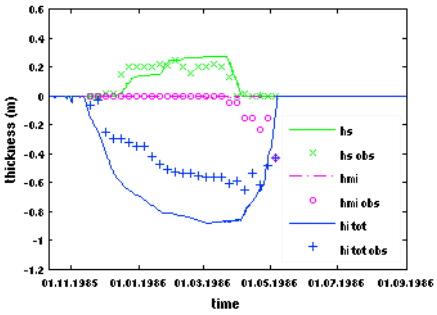

Fig. 8. Observations and model simulation at Ajos station in 1985--1986.

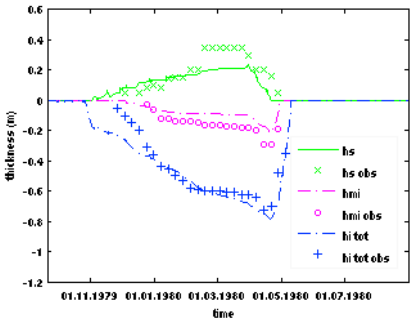

Fig. 9. Observations and model simulation at Ajos station in 1979--1980.

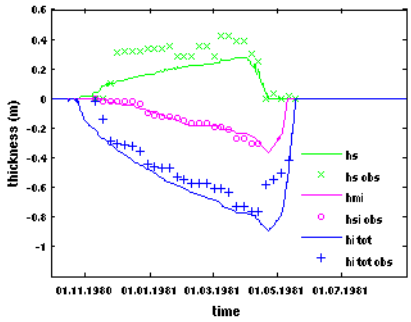

Fig. 10. Observations and model simulation at Ajos station in 1980--1981.

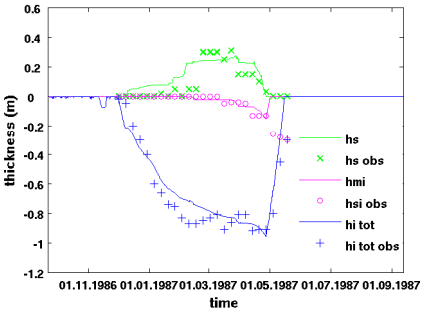

Fig. 11. Observations and model simulation at Ajos station in 1986--1987.

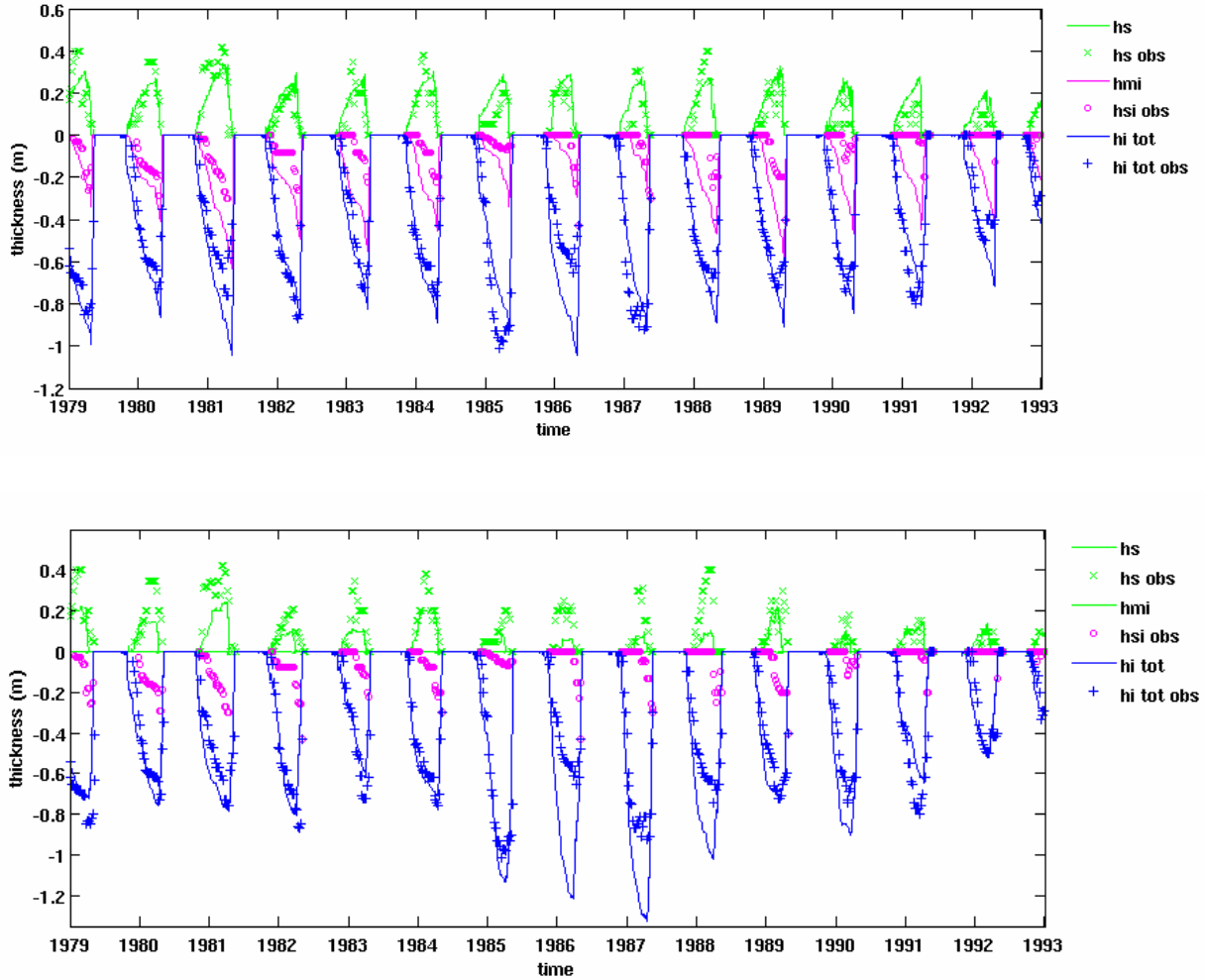

Fig. 12. Sensitivity of the model to increased (above) and decreased (below) precipitation (Ajos).